them. Such objects introduce many difficulties that have not been addressed in this work, including incomplete cross-sections and non-parallel surface cuts of primitives, especially at joints. More generally, the problem lies in the non-observability of geometric projective properties due to structural events. We believe, however, that the constraints and the methods developed here will be an important part of handling those objects. The resulting structured descriptions have applications in 3-D shape from 2-D contours and recognition.

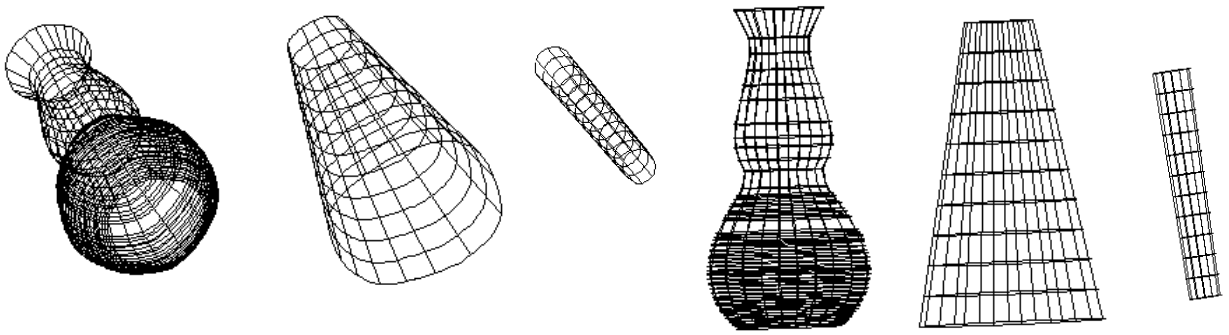

a.

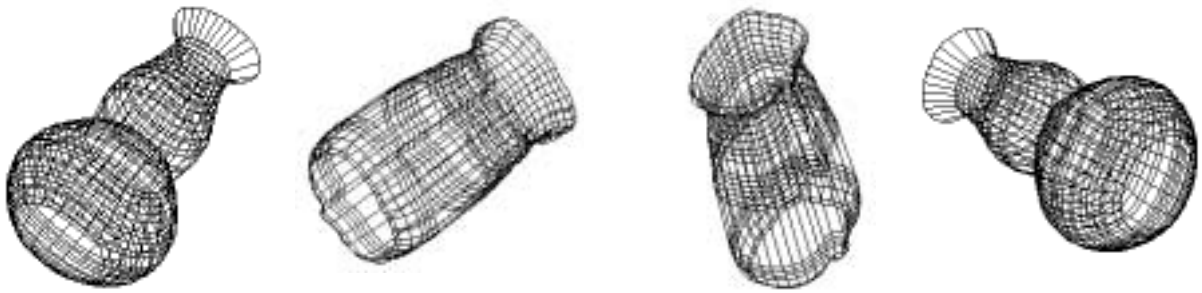

b.

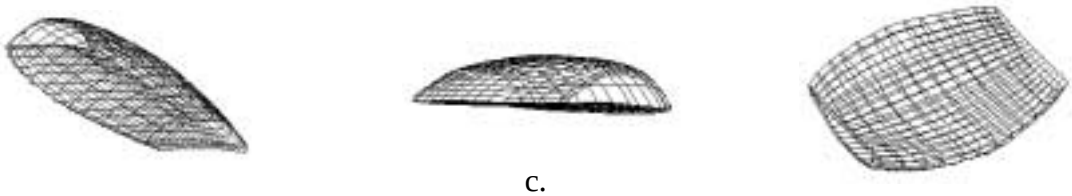

c.

Figure 9.2 Recovered 3-D descriptions of previous SHGC scenes shown for different poses. a. from figure 7.12. b. from figure 7.13 . c. from figure 7.13 (continued)

they are incomplete. We have also demonstrated the usage of our results for 3-D shape recovery, using a single image of a scene.

We hope to extend this approach to handling composite objects made up of straight and curved axes primitive GCs. These two types of primitives, when combined, generate a large class of objects such as industrial parts and animal shapes. We have recently analyzed projective quasi-invariant properties of a large class of curved axis GCs and derived a method to recover their 3-D shape from 2-D contours in [Zerroug 1993b, 1993c]. Detection of composite objects can proceed by detecting the component GCs and analyzing structural and geometric relationships between

projection of the SHGC axis. Let I' = (OW, x', y') be obtained by rotating I by θ. Then, in I' the SHGC axis is horizontal, and S' and W' differ only by a translation OS-OW. The relationship between coordinates in S, S', W' and I' are as follows (we will henceforth omit the arguments t and s in the expressions):

Letting $(x_S, y_S, z_S)^t$ be the coordinates of OS in W' (see Figure 9.1), a point P with coordinates $(ru, rv, s)^t$ in S has coordinates $(\cos\sigma\, ru + s \sin\sigma, rv, -\sin\sigma\, ru + s \cos\sigma)^t$ in S', $(\cos\sigma\, ru + s \sin\sigma + x_S, rv + y_S, -\sin\sigma\, ru + s \cos\sigma + z_S)^t$ in W' and its projection has coordinates $(\cos\sigma\, ru + s \sin\sigma + x_S, rv + y_S)^t$ in I'. In the remainder of this analysis, we consider image measurements in I'. World coordinates will be expressed directly in W'.

To recover a complete 3-D description of the SHGC, it is necessary to determine the 3-D top cross-section, the orientation of the axis, the coordinates $(x_S, y_S, z_S)^t$ of its origin (point where the axis pierces the cross-section plane, not necessarily at its center) and the values s_i (i = 1..n) (call them s-values) of the cross-sections (parallels) of interest. The recovery of those parameters is discussed in Appendix B.

Application of this method to the descriptions obtained in Figure 7.12 and Figure 7.13 is shown in Figure 9.2, where the objects are displayed for different values of slant and tilt from the objects' original pose. The figure shows the 3-D ruled surfaces in terms of cross-sections and meridians. At this stage, complete 3-D object centered descriptions of the viewed objects are recovered.

10 Conclusion

We have presented an approach to scene segmentation and shape description in real monocular images containing objects that can be described as SHGCs. Two important aspects characterize our method. First, we have derived (and used) important projective invariant properties of SHGCs. Second, the method is based on feature grouping using rigorous constraints derived from those projective invariant properties. It addresses the figure-ground problem throughout a hierarchy of three feature levels, where it not only filters out irrelevant features (not satisfying the properties) but detects where relevant ones are missing and completes them adequately. The projective invariant properties are the basis for detecting local descriptions, hypothesizing groupings, estimating more accurate global descriptions, verifying their global consistency and completing them if

obtained by applying the method of [Ulupinar 1990a] on our results. For this, we assume that we have a Right SHGC (i.e. $\alpha = \pi / 2$ in equation (3.1)). This equation becomes:

$$S(t, s) = (r(s)\, u(t), r(s)\, v(t), s) \tag{9.1}$$

Without loss of generality, we assume that $s = 0$ for the top cross-section and that $r(0) = 1$ (the scaling is relative to the top cross-section). Note that our 2-D description already provides the values $r(s_i)$ (the scaling is an *orthographic invariant*). However, it does not provide the values s_i necessary for a complete description of the sweeping function.

Figure 8.2 gives the configuration of the coordinate systems relevant to this analysis. We denote $S = (OS, u, v, s)$ the SHGC coordinate system, $W = (OW, x, y, z)$ the viewer coordinate system and $I = (OW, x, y)$ the image coordinate system. Without loss of generality, we assume that the viewing direction $\vec{V}$ (orthographic projection assumed) lies in the *u*-*s* plane of the SHGC coordinate system. $\vec{V}$ makes an angle σ with the *s*-axis (SHGC axis). Consider $S' = (OS, u', v', s')$ ob-

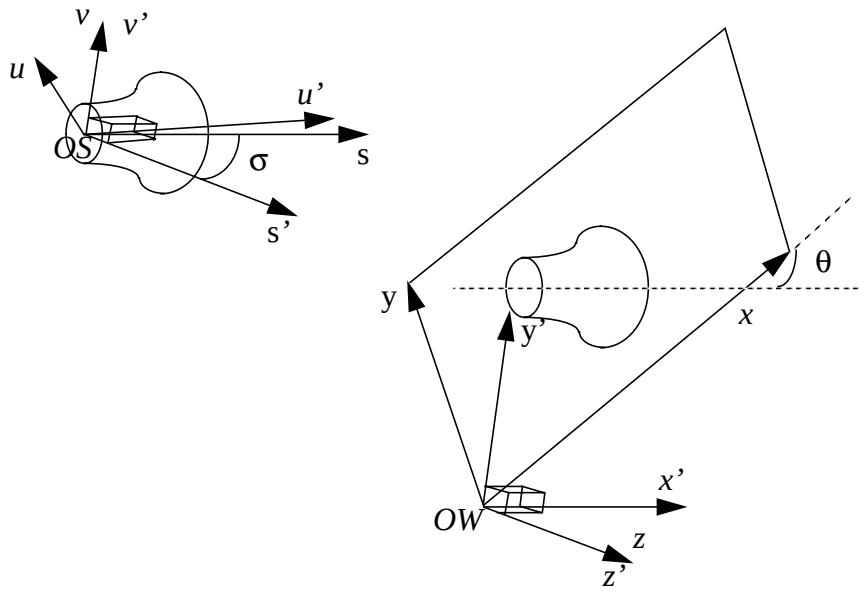

Figure 9.1 SHGC representation and projection geometry

tained by rotating *S* around *v* by σ so that the new *s*-axis *s'* is aligned with $\vec{V}$.

Let θ be the angle between the projection of the SHGC axis and the *x*-axis. Consider $W' = (OW, x', y', z')$ obtained by rotating *W* by θ around *z* so that the new *x*-axis, *x'*, is parallel to the

11. by parameters, it is meant the set $\{C, A, S\}$ given in the definition of an SHGC.

local SHGC patches compared to 94 for the default values. Most importantly, the same final results have been obtained by changing the values of the parameters, which for the case of Figure 1.1 are one grouping hypothesis and two terminations (selecting 4 local SHGC patches from the 94 originally hypothesized), resulting in the last three SHGCs given in Figure 7.12.

By way of comparison, the method of Sato and Binford [Sato 1992a and b] is similar to ours in the principle of using projective invariants to detect SHGCs. It differs, however, in two ways. First, application of the projective properties in their method is somewhat restricted to surfaces of revolution (SORs) and LSHGCs. Their application of the properties to surface detection, for example, may not give accurate results for general SHGCs as limb projections are generally *not* meridian projections. For example, in their system, correspondence segments between limbs are assumed to be parallel, whereas it can be shown that this is not the case in general (this is true for SORs and LSHGCs). We also believe that our application of the properties is more robust. For example, their parallel symmetry detection uses a Hough transform to detect the point of intersection of correspondence lines between symmetric curves. For symmetries with a scaling factor close to 1, the error in the detected point can be large. We use property 5 which is less sensitive to errors in correspondences as such errors cause only small changes in length ratios and directions of corresponding segments.The main difference between their method and ours, however, lies in handling occlusion and large gaps. The authors note that their system does not handle occlusion as boundary connectivity criteria are used for surface detection. Our SHGC patch level grouping handles breaks and occlusion by detecting visible local surface patches and grouping of compatible ones into global surface descriptions. Further, our method also detects non-visible parts of the objects and completes them adequately thereby producing complete surface descriptions.

9 Application to 3-D Shape Recovery

In this section, we discuss the application of our obtained results to 3-D shape recovery. Previous work on 3D shape recovery of SHGCs [Ulupinar 1990a] assumed that perfect and segmented boundaries were given. The results of our segmentation method do provide the required descriptions for that method. However, that method recovers only a viewer-centered description giving the 3-D surface normals at visible sections of each object surface. In many applications, however, it is desirable to have a complete object centered description, also providing volumetric information. For this, we propose a method that recovers the 3-D parameters[11] of an SHGC. The method consists of using constraints from both our 2-D descriptions and the 3-D viewer-centered descriptions

is straightforward as all such descriptions involve the same cross-section, same axis and same scaling function. It can be easily seen that, for detecting presence of such an object, it is not necessary to consider all such limb boundaries. Any pair would be sufficient for detection of the object and its 3-D recovery since the properties of section 3 apply regardless of whether the cross-section is concave or convex. The hypothesis merging step, however, allows to have a better segmentation by identifying all observed contours belonging to the same object.

Also, we have stressed that the method handles occlusion and this is shown in the example of Figure 1.1 and the images of Figure 7.13 and Figure 7.13 (continued), where important object boundaries are hidden by other objects.

This method shows the relevance of the projective invariants (those we have derived and others) for solving the figure-ground problem. However, since the method is based on hypothesizing presence of SHGCs using evidence from those projective invariant properties, it fails when such properties are not observed in the image. For example, cross-sections may not visible in the case of composite objects due to joints between components. This work does not address such compound objects but simple objects which can be described as SHGCs. Difficulties related to the effects of joint patterns on observability of projective invariants and structural events are currently being studied in the context of a more general approach for handling compound objects, in real images, made up of both straight axis primitives, such as SHGCs, and curved axis ones. We have already studied projective properties of primitives having curved axis and varying cross-section size, such as horns for example. In [Zerroug 1993a], we derive important projective *quasi-invariant* properties of such primitives and show how they can be used to recover 3-D shape from 2-D contours.

A number of parameters have been used in the implementation of our system. We have mentioned them throughout the description of the method. For example, connection measures in the parallel symmetry level, linearity of limbs and axes and junction measures in the SHGC patch level. In all the tested images, the values of all parameters have been constant. Robustness of the system to changes in those parameters has been tested by changing their values by 50% of their default ones. Those changes have only affected the number of hypotheses and consequently the size of the search space. Looser thresholds produce larger search spaces. In the case of the contours of Figure 1.1, for example, increasing the values of the connection measures of the parallel symmetry level by 50% of their default ones produced 17 connection hypotheses compared to 4 for the default values. Also, changes by 50% of the linearity thresholds, in the SHGC patch level, produced 95

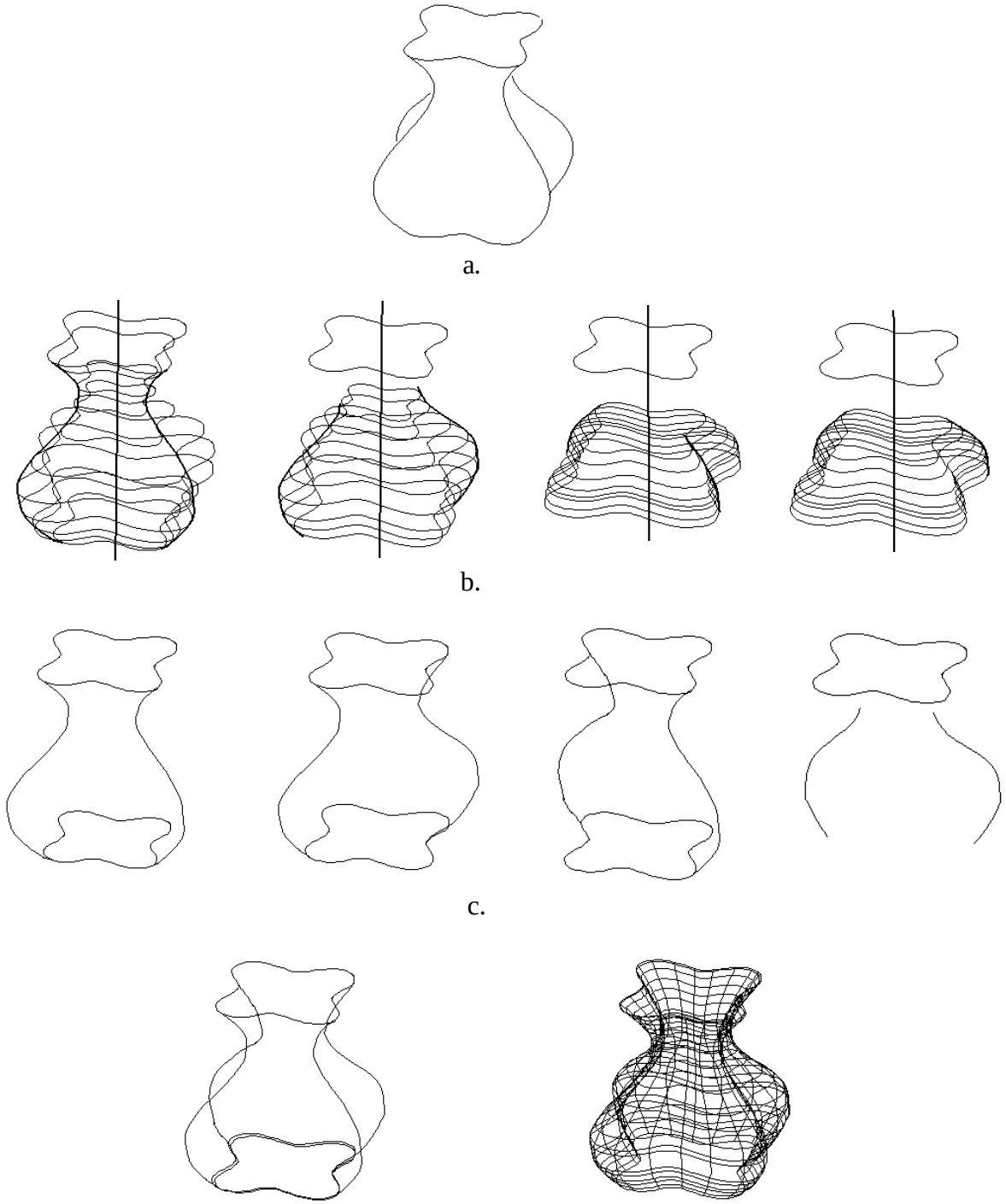

Figure 7.14 Multiple (merged) hypotheses that correspond to the same SHGC object. a. original boundaries. b. all detected local SHGC patches. c. completed descriptions (and contours). d. resulting global SHGC description.

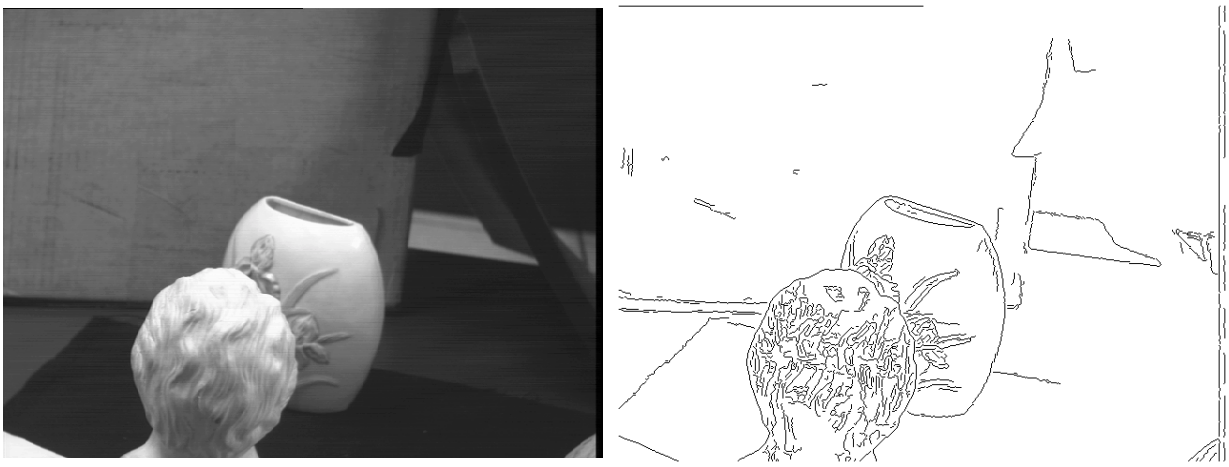

a.

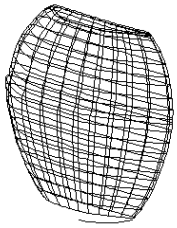

b.

Figure 7.13 (continued)Another scene involving a different SHGC occluded by a non-SHGC object. a. original intensity image and extracted contours. b. final result.

ods we have given in section 3 (*a fortiori*) apply to meridian projections. For example limb correspondences for local SHGC patch detection can still be determined in the same way we have discussed. In fact, some the methods are even simplified in cases sharp edges exist. For example, limb reconstruction of a sharp edge consists simply of tracing the recovered cross-sections corners. In the image of Figure 7.13 (continued), for example, the occluded SHGC has such an edge at the right side but a limb boundary at the left side (the back side of the cross-section is straight). Furthermore, the method also applies to cases where the cross-section has concavities which create several discontinuous limb boundaries through self-occlusion. Such an example has been shown in Figure 7.14. The SHGC detection is achieved in the same way as though the discontinuities produced by self-occlusion were caused by occlusion from another object. The only difference with other types of SHGCs (with convex cross-section, for example) is that several verified hypotheses will result for the same object. Identification of such a case, as mentioned at the end of section 7.5,

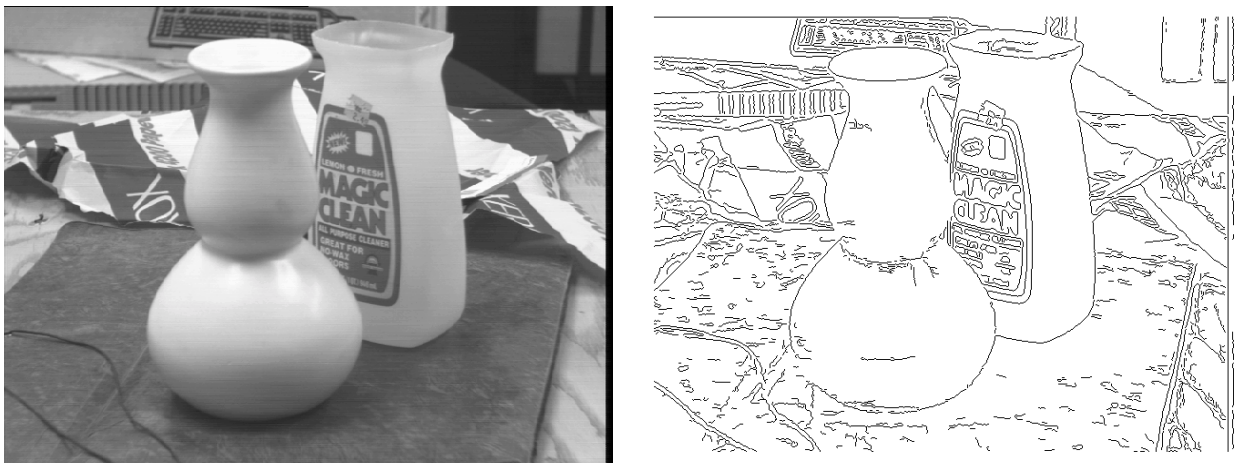

a.

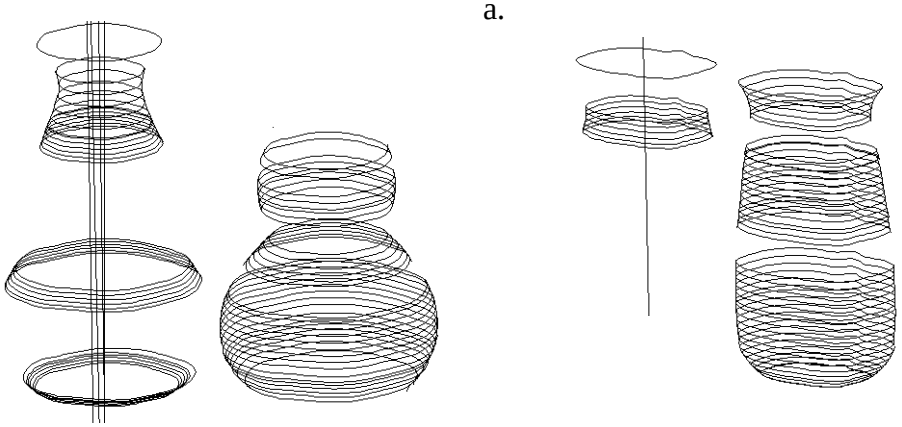

b.

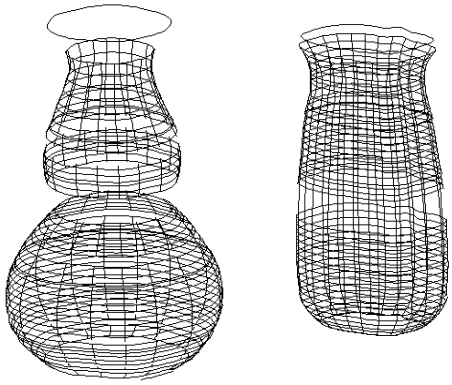

c.

Figure 7.13 *Other examples of the application of the segmentation method.* a. *original intensity image and extracted contours.* b. *component patches of the segmented objects and the corresponding completions (only the verified hypotheses are shown).* c. *complete descriptions of the segmented objects.*

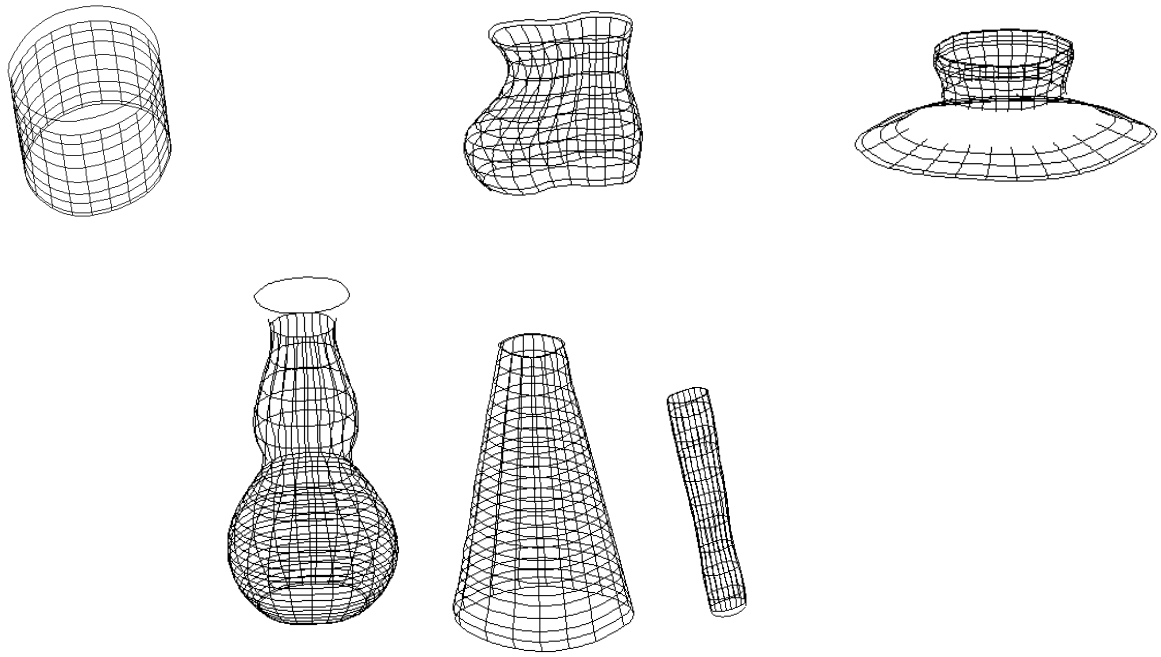

c.

Figure 7.12 (continued) c. Ruled surfaces

8 Discussion and Comparison

We have tested our method on several images and satisfactory results have been obtained. Some of the simple examples have been presented here so as to illustrate the different steps of the method. The others involve multiple objects in different arrangements such as the last example in Figure 7.12a (from the intensity image of Figure 1.1) and those of Figure 7.13 and Figure 7.13 (continued). The method we have presented is not limited to special types of cross-sections nor does it assume bilateral symmetric limb boundaries. The SHGC in the middle of the first row of Figure 7.12 is an example of non-circular cross-section SHGC, as are the occluded objects in both images of Figure 7.13 and Figure 7.13 (continued) and the object of Figure 7.14. The method also handles cross-sections with tangent discontinuities which create sharp edges over the surface. The only difference between such edges and limb boundaries is that the former are the trace of a single point of the cross-section (thus, meridians) whereas the latter are not. All the properties and meth-

a.

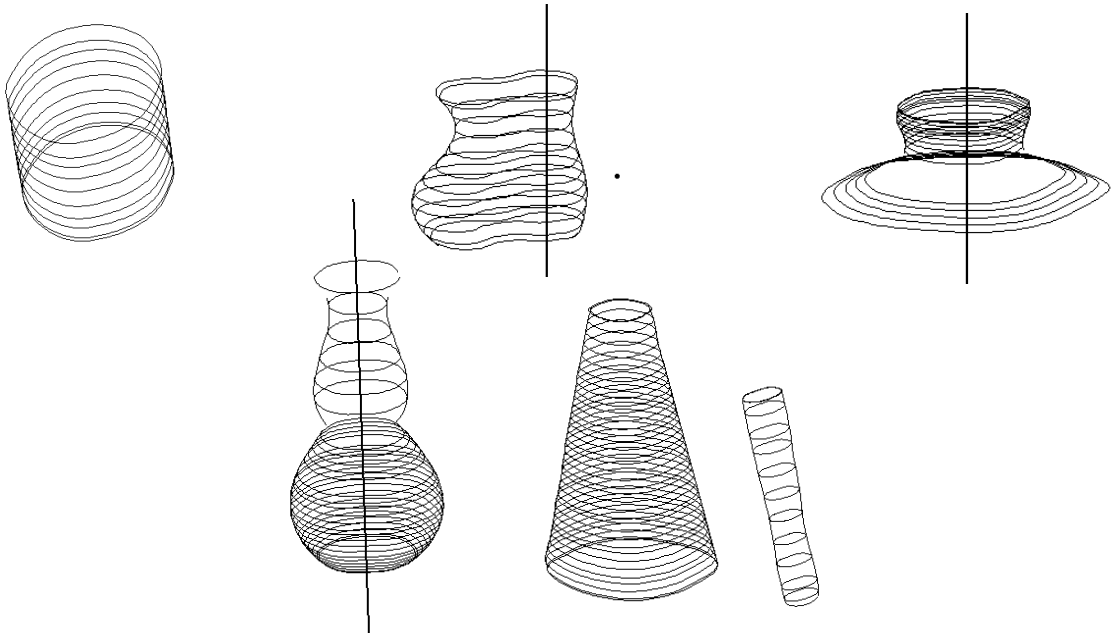

b.

Figure 7.12 Results obtained in level 3. a. Original contours. b. Obtained global SHGCs. c. Ruled surfaces.

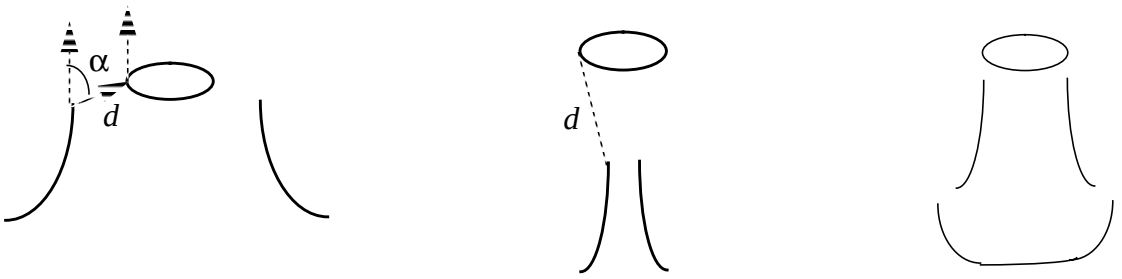

non closed object non closed object closed object

igure 7.11 Closure verification.

Results of this level on the objects shown previously are given in Figure 7.12 and Figure 7.12 (continued). Figure 7.12.*a* shows the original contours. The last example is from the intensity image of Figure 1.1. Figure 7.12.*b* shows the detected global SHGCs. Recovered cross-sections and axes are shown. Figure 7.12 (continued).*c* shows the ruled surfaces (recovered cross-sections and meridians). Figure 7.13 and Figure 7.13 (continued) show some more examples of results applied to other images also involving other objects with different occlusion patterns and background texture and markings. Figure 7.13.*b* shows the detected local SHGC patches that belong to the final segmented objects and the recovered completions (as discussed in section 7.5).

Resulting global SHGC descriptions usually each correspond to a single and different object in the scene. However, it may happen that several hypotheses point to the same object. This might be the case of an SHGC with a concave cross-section and whose surface has several limb boundaries which exhibit complex self-occlusion patterns. Our method detects local SHGC patches for each pair of such limbs and completes discontinuous descriptions as though self-occlusions were caused by other objects. Thus, several SHGC patches will be detected for such an object, but all correspond to the same SHGC (same hypothesized cross-section, same axis and scaling function). A *hypothesis merging* step is performed on such hypotheses to yield one global SHGC description involving all the hypothesized patches and their (completed) limbs. Figure 7.14 shows an example of such complex SHGC and the results obtained by our method. Figure 7.14a shows the original boundaries (notice the self-occluded limb patches). Figure 7.14b shows detected local SHGC patches involving different pairings of limb patches (displayed in thick lines). Figure 7.14c shows the corresponding completed descriptions (notice the completed limb patches that were occluded in Figure 7.14a). Figure 7.14d shows the final (merged) SHGC description showing the complete ruled surface of the detected object.

tions, the method essentially treats the infinitesimal patch between two successive cross-sections as being an LSHGC patch (where line tangents and limbs are colinear; i.e. Property P2).

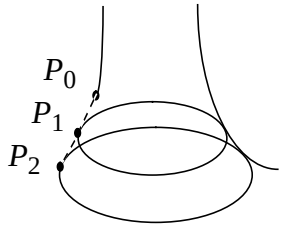

Figure 7.9 Limb reconstruction method.

For LSHGCs the limb reconstruction is straightforward as it only consists of extending the known straight limbs for continuous or discontinuous connections (or terminations). For discontinuous connections of a non linear SHGC, the boundary completion is not performed as no cross-sections could be recovered for the holes mentioned previously. However, the SHGC can still be used for 3-D shape recovery and recognition (the hole region will be left unspecified).

Figure 7.10 shows the limb boundaries so completed for the SHGCs of Figure 7.8.

Figure 7.10 Limb reconstruction for the SHGCs of Figure 7.8.

Completed SHGCs are further verified for closure. Closure verification consists of checking required junction properties for the global SHGCs. Using the terminology used in [Malik 1987], limb curves and the *top* cross-section generally form *three-tangent* junctions[10]. At the *bottom* cross-section, they form *curvature-L* junctions. Because junctions cannot be expected to be perfect in real image contours, we use measures based on proximity and angular variations at limb extremities and matching points on the top cross-section or end points of the bottom cross-section. Figure 7.11 shows some examples. Hypotheses with non closed objects are rejected.

10. in the case of edges (non limb boundaries) arrow and Y junctions are formed.